Influence of the Side Branch Structure Pattern of the Imitation Cat's Claw Function on the Vibration and Noise of Tires

Guolin Wang[1] – Kexin Zhu[1] – Lei Wang[1] – Jian Yang[1],* – Lin Bo[2]

[1] Jiangsu University, School of Automotive and Traffic Engineering, China
[2] KENDA Industrial Co., Ltd, China

To study the method of reducing the low-frequency vibration noise of tires, a passenger car tire (205/55R16) is taken as the research object. The dynamic grounding characteristics and vibration reduction mechanism of the cat's paw pad are analysed. The research showed that the swing deformation characteristics of paw pads during the walking process of cats are one of the main ways to reduce the impact from the ground and achieve vibration reduction and silencing. To analyse the influence of tire grounding on noise, tire grounding is divided into five areas, and the characteristics of ten tire grounding areas are analysed through tests. Pearson correlation analysis is used to obtain the characteristics of the eight most relevant grounding parameters with tire noise, and multiple linear regression is conducted between the characteristics of the eight grounding areas. The product of the correlation coefficient and the average value of the characteristics of the ground contact area shows that the central area of the tire tread contributes the most to the tire noise. The swing deformation characteristics of the bionic cat paw pad are realized by setting the staggered side branch pipe groove in the centre of the tire, and the vibration reduction characteristics of the bionic tire are analysed using the finite element method. The results showed that when the tire rolls, the amplitude and fluctuation range of the ground radial excitation force acting on the bionic tire are reduced compared with the original tire, and the vibration and noise characteristics of the tire are improved.
Keywords: bionics, vibration damping mechanism, vibration noise, tread pattern, structural design

Highlights
- *The swing deformation characteristics of paw pads during the walking process of domestic cats are one of the main ways of reducing the impact from the ground and achieving vibration reduction and silencing.*
- *The relationship between the tire grounding characteristic parameters and the measured noise is studied by region, and it is concluded that the tire tread centre area contributes the most to the tire noise.*
- *The dynamic and acoustic models of the tire are established and verified.*
- *The bionic design of the tread pattern in the centre of the tire tread was carried out, and the noise reduction mechanism of the bionic tire is analysed regarding the radial excitation force and noise of the tire.*

0 INTRODUCTION

Road traffic noise has become a significant source of noise pollution [1]. Studies have shown that when the driving speed of the car exceeds 70 km/h, the tire noise will become the main part of the vehicle's noise, accounting for more than 30 % of it [2]. In recent years, the tire labelling laws implemented in the European Union, the United States (US), and other countries and regions have put forward strict requirements on tire noise performance [3]. The vibration and noise of tires are one of the main reasons that affect the noise, vibration, and harshness (NVH) performance of vehicles [4] and [5]. How to reduce tire vibration and noise has always been the focus of major tire manufacturers. Ji and Bolton [6] analysed the relationship between tire vibration characteristics and radiated noise by using the structural modal analysis method. The results show that low-order modes have a greater impact on tire vibration radiated noise, and the frequency corresponding to the peak sound pressure is often near the natural frequency of the tire.

Through simulation and experimental analysis, Zuo et al. [7] concluded that the periodic collision between tread blocks and the road surface is the main source of tire vibration noise, and the collision frequency is closely related to the number and size of blocks. Mohammadi and Ohadi [8] proposed a new method of reducing tire noise by using the multi-objective minimization method, optimized the structure and tread pattern parameters of patterned tires, reduced tire noise, and provided ideas for the research of low-noise tire patterns. Pei et al. [9] determined that the tread is the component with the greatest contribution to the tire by studying the contribution of each part of the tire's outer contour to vibration and noise and adding polyester damping materials to the tread and sidewall to suppress tire vibration. Zhang et al. [10] tested and compared the tire noise of different tire carcass structures. The results showed that the types and layers of carcass skeleton materials would change the vibration state of the carcass, thus affecting the tire noise. Although these noise reduction methods have achieved certain effects, in the finite element

*Corr. Author's Address: Jiangsu University, School of Automotive and Traffic Engineering, Zhenjiang, China, yangjian@ujs.edu.cn

49

analysis process, only smooth tires or tires with only longitudinal grooves are mostly used, and complex patterns are not considered. However, in the actual driving of passenger cars, most use complex tread patterns, and the vibration noise at low speeds is mainly caused by the tread patterns hitting the ground [11], so it is essential to study low-noise tread patterns.

In long-term biological evolution, animals have formed super-adaptive abilities to nature. The extremely strong vibration damping and muted effect of cats in the process of walking and running have long been a research focus of scholars. The paw pad of a domestic cat is the only body part that contacts the ground, which plays a very important role in the vibration reduction and silence of the domestic cat during walking, running, and jumping. Coulmance et al. [12] measured the forces exerted by the limbs of the cat during walking. The results showed that the front paw lift was preceded and accompanied by postural adjustment and that the front paws had a more important role in the cat's postural adjustment. Zhang et al. [13] established a mass-spring model to simulate the landing behaviour of domestic cats after jumping and used this model to analyse the cushioning characteristics of the domestic cat's paw rest. Kruger et al. [14] used a high-frequency camera to capture images of domestic cats and wild cats during normal walking, sprinting, and jumping from a height, and compared and analysed the cats' limb movements in different states.

With the deepening of research, the concept of bionics has been integrated into all walks of life and has been used as an important means of technological innovation. Wang et al. [15] applied the arc structure of the locust's foot in nature to the tread arc design of the tire, which reduces the tire wear and enhances the grip ability of the tire while reducing the vibration noise of the tire. The Gubo Tire Company and Polymer Research Center in Madison, Wisconsin, USA jointly developed a kind of non-pneumatic military honeycomb-like tire, which has good shock absorption and defence characteristics [16].

Chen et al. [17] can quickly disperse the boundary layer vortex with the help of the non-smooth structure of shark skin, so as to improve the principle of water flow speed. The non-smooth structure is set at the bottom and wall of the tire ditch to improve the tire's water-skiing performance. Zhang et al. [18] established a mathematical model of reindeer foot characteristics with the help of the reindeer's strong grip when walking on ice, and a bionic design was carried out for the tire tread. The bionic tire increased the contact area with ice and improved the anti-skid

performance of the tire. Zhou et al. [19] were inspired by the strong adsorption capacity of octopus suction cups and established three bionic concave funnel suction cup tire patterns. Through simulation analysis, the bionic patterns have better tensile and compressive properties and better adsorption capacity on the ice surface, ensuring the anti-skid ability of the tire on the ice surface. With in-depth research on the mechanism of biological characteristics, such traits can be more reasonably applied to various industries. In order to apply the strong vibration reduction and mute effect of domestic cats when walking, running, and jumping to the design of a low-noise tread pattern structure, it is necessary to study the vibration reduction and mute mechanism of domestic cats to guide the structural design of low-noise tread pattern.

This paper takes the 205/55R16 tire as the research object and studies how to reduce the low-frequency vibration noise of the tire. The dynamic grounding characteristics and vibration reduction mechanisms of domestic cat paw pads are analysed, and the bionic noise reduction modification design of the tread pattern is carried out. The shock absorption characteristics of the imitation cat paw pad are realized by setting a staggering side branch pipe groove in the central area of the tire. On this basis, the noise reduction mechanism of imitation domestic cat paw pad pattern tires is studied.

1 A STUDY ON THE VIBRATION REDUCTION MECHANISM OF CAT PAW PADS

1.1 Mechanical Experiment of Contact Between Claw Pad and Ground

The purpose of the mechanical test on the contact between the paw pads of domestic cats and the ground is to obtain the vertical reaction force and strain characteristics of the paw pads of domestic cats in normal walking gait (v = 0.4 m/s to 0.8 m/s). The subjects are two healthy, defect-free domestic cats, aged 6 years, weighing 4.5 kg and 4.7 kg respectively. During the test, a pressure-sensitive channel (walkway A101; (Tekscan, USA)) is used to measure the vertical reaction force generated when the paw pads of domestic cats pass straight over the pressure plate at different speeds. To obtain the strain characteristics of the domestic cat on the ground, when the domestic cat walks in a straight line on the glass plate, grey speckles are added to its foot pads, as shown in Fig. 1. The motion of the paw pads was recorded by a high-speed camera (Olympus i-SPEED) installed under the glass plate, and then the images are digitized using the

VIC-2D of CSI Company (USA) to obtain the strain and related information of the paw pads in contact with the ground.
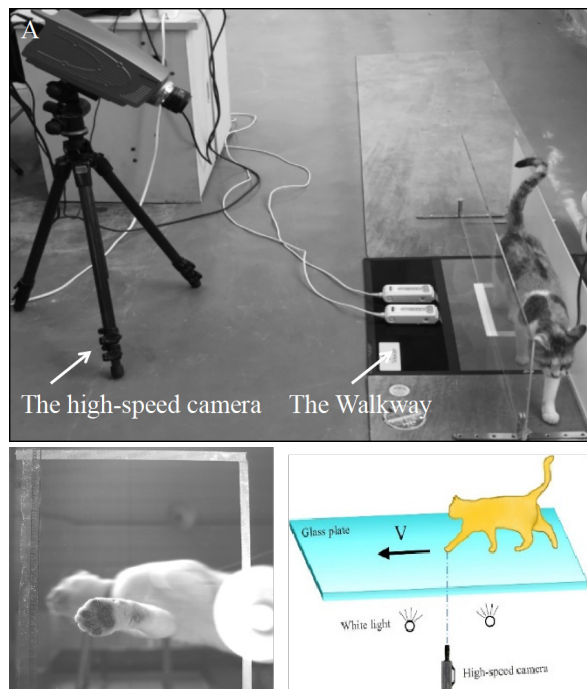
Fig. 1. *The contact tests of paw pads; a) contact pressure test; b) contact strain test*

1.2 Mechanical Analysis of Contact between the Claw Pad and the Ground

The contact strain magnitude and direction data information between the cat paw pad and the ground is obtained through VIC-2D digital processing. Relevant research [12] and [20] shows that when dogs and cats exercise, their front paw pads always play a more critical role than their rear paw pads in the process of realizing biological functions. Therefore, this paper mainly considers the front paws of cats. The three groups of effective tests are selected for analysis of the two domestic cats, and the strain characteristics with the same trend were obtained. This paper takes the centre group as an example to analyse the strain characteristics. The magnitude and direction of the contact strain between the palm pad and the toe pad are shown in Fig. 2. In the figure, the X direction is the forward direction of the cat, and the Y direction is the inner side of the cat's paw pad. From the principal strain direction, the deformation direction of the toe pad area has no change, and it is always tensile deformation in the Y direction. Before

0.180 s, the tensile deformation of the palm pad area is mainly in the Y direction, and after 0.180 s, the tensile deformation in the X direction is mainly in the X direction, which indicates that the swing deformation characteristics of the palm pad area exist in the X and Y directions. From the perspective of principal strain, the principal strain values of the four toe pads increase continuously during the whole contact process. The strain value of the pad increases first and then decreases alternately in the inner and outer regions. The maximum principal strain of the palm pad is significantly lower than that of the toe rest, which is caused by the change in the strain direction. This further illustrates that the palm pad area has the characteristics of swing deformation, vibration reduction, and noise reduction in the process of contacting the ground.
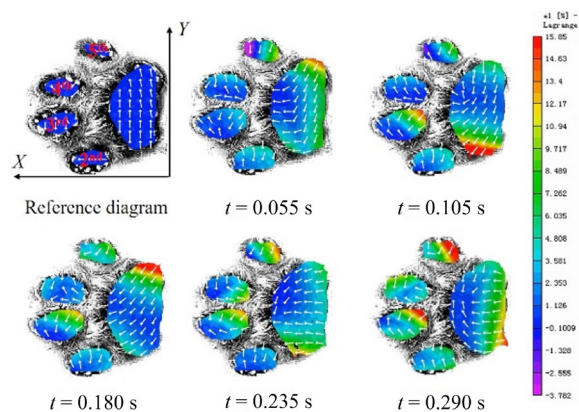
Fig. 2. *Strain magnitude and direction of contact between claw pad and ground*
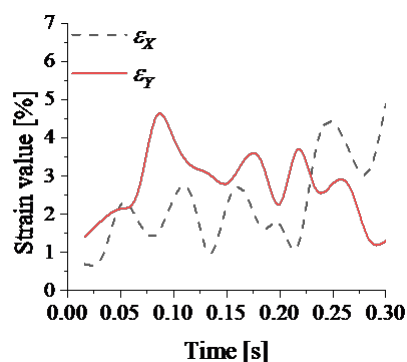
Fig. 3. *Time domain diagram of contact strain in X and Y directions of palm pad area*

To further clarify the attenuation of the strain value during the contact between the palm pad and the ground, the strain values in the X and Y directions of the palm pad area during the entire grounding process are extracted and plotted as a curve of the

strain value changing with time, as shown in Fig. 3. During the whole grounding process, the strain value of the palm pad area reflects a fluctuation change law with the opposite trend in X and Y directions, and the strain value of the palm rest is attenuated during the fluctuation process, which further proves that the impact load on the palm rest area during the grounding process can realize some dissipation with the swing deformation in X and Y directions.

2 TIRE GROUNDING DEFORMATION CHARACTERISTICS TESTING AND ANALYSIS

2.1 Tire and Ground Pressure Distribution Testing

Fig. 4 is a physical map of 205/55R16 PCR tires produced by 10 different manufacturers and used in this experiment. Table 1 lists the noise-related information of 10 test tires. The noise values are derived from the tire performance test data published in the literature [21]. In this paper, the noise performance of the tire is evaluated with the pass-by noise, which is the noise value measured by the test tire when the vehicle's engine is turned off and the vehicle passes through the measurement area at a speed of 80 km/h.

Fig. 4. *Physical drawing of 205/55R16 test tire*

Table 1. *Test tire information and noise value*

Number	Type	Through noise value [dB]
1	Turanza ER 300	71.5
2	PROXES C100 PLUS	71.5
3	LS388	71.0`
4	MARMONIC M220	70.4
5	ADVAN dB DECIBEL V551	71.1
6	SPORT SA-37	72.1
7	Primacy 3 ST	70.6
8	N'FEAR SU4	70.8
9	Efficient Grip Performance	70.7
10	Conti Max Contact MC5	72.4

As shown in Fig. 5, the American Tekscan pressure test system is used to obtain the grounding marks and pressure distribution of 10 test tires. The inflation pressure of the tires during the test is 0.24 MPa of the rated pressure, and the load is 4821 N of the rated load.
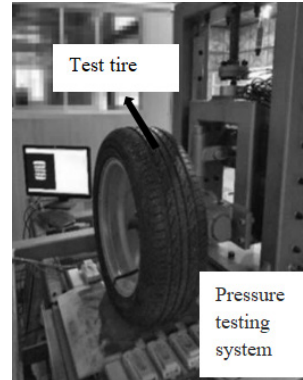
Fig. 5. *Ground pressure deformation*

2.2 Grounding Area Division and Grounding Parameters

Most of the 10 tires used in the test have asymmetric tread patterns and are divided into five areas by four longitudinal grooves. Therefore, the tread is divided into five areas by taking the groove wall of four longitudinal grooves as the boundary: the outer shoulder area (I), the outer transition area (II), the central area (III), the inner transition area (IV), and the inner shoulder area (V).
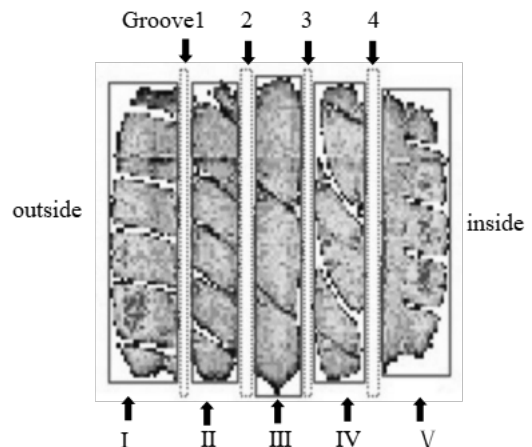
Fig. 6. *Tread grounding area division*

The ground deformation parameters are mainly divided into grounding geometric parameters and grounding pressure parameters. The geometric parameters are the grounding area, imprint area, grounding area ratio, grounding length, grounding

width, grounding aspect ratio, and rectangle ratio. The pressure parameters are average grounding pressure and grounding pressure skewness. Liang [22] defines the grounding geometric parameters and grounding pressure parameters of tires in detail. Through the test, the grounding geometric parameters and grounding pressure parameters of the whole area of the grounding footprint, the outer tire shoulder area (I), the outer transition area (II), the central area (III), the inner transition area (IV), and the inner tire shoulder area (V) are divided into 54 grounding deformation characteristic parameters.

2.3 Analysis of Grounding Deformation Parameters

Due to the limited number of test tires and the need to find evaluation indexes related to high noise value, the Pearson correlation analysis method is used to eliminate the ground deformation parameters with poor correlation with noise value; it is calculated as follows:

$$r = \frac{\sum_{i=1}^{n}(x_i - \bar{x})(y_i - \bar{y})}{\sqrt{\sum_{i=1}^{n}(x_i - \bar{x})^2 \sum_{i=1}^{n}(y_i - \bar{y})^2}}. \quad (1)$$

In the formula, n is the number of samples. y_i, $\bar{y}$, x_i, and $\bar{x}$ are the tire noise value, the average tire noise value, the tire grounding parameters, and the average grounding parameters, respectively.

The correlation level is evaluated by the significant coefficient. The formula of the significant coefficient is:

$$t = \frac{r\sqrt{n-2}}{\sqrt{1-r^2}}, \quad (2)$$

where t obeys the t distribution with $n - 2$ degrees of freedom.

When $|r| > 0.5$ and $t < 0.05$, the ground deformation parameter is highly correlated with the noise values. Through the analysis of 54 grounding deformation characteristic parameters mentioned in Section 2.2, the grounding deformation characteristic parameters ($|r| > 0.5$ and $t < 0.05$) related to high noise value are obtained, as shown in Table 2.

Table 2. *Grounding parameters related to high pass-through noise*

Area	Grounding parameters	Noise value	
		r	t
the overall area	Rectangle ratio (x_1) [%]	−0.674	0.033
	Average ground pressure (x_2) [kPa]	0.855	0.002
	Deviation value of grounding pressure (x_3) [kPa]	0.677	0.031
the outer shoulder area (I)	Grounding length (x_4) [mm]	−0.853	0.002
the central area (III)	Average ground pressure (x_5) [kPa]	0.750	0.012
the inner transition area (IV)	Average ground pressure (x_6) [kPa]	0.788	0.007
	Deviation value of grounding pressure (x_7) [kPa]	0.705	0.023
the inner shoulder area (V)	Grounding length (x_8) [mm]	−0.744	0.014

The quantitative relationship between the grounding deformation characteristic parameters and the noise value can be obtained through multiple linear regression, and the contribution of each parameter and region to the noise value can be clearly obtained through the formula. Table 3 shows the ground deformation characteristic parameter values related to high noise corresponding to 10 tires. Taking Table 3 as the multiple linear regression sample, the relationship between the noise value and the grounding deformation characteristic parameters obtained through multiple linear regression is:

Table 3. *Sample scheme by noise value*

i	x_1	x_2	x_3	x_4	x_5	x_6	x_7	x_8	Noise value, y [dB]
1	0.868	376.368	183.461	118.667	364.899	396.095	188.851	112.667	71.5
2	0.891	365.712	181.264	115.667	349.691	411.347	174.922	112.000	71.5
3	0.919	379.622	192.799	124.000	354.681	381.658	188.859	116.000	71.0
4	0.871	350.895	166.829	132.000	348.677	383.964	177.211	124.667	70.4
5	0.925	375.085	186.990	131.667	365.922	411.568	163.246	115.000	71.1
6	0.867	394.792	179.938	113.000	416.636	428.593	182.123	109.333	72.1
7	0.909	342.809	160.781	125.333	319.412	382.447	172.136	113.333	70.6
8	0.909	373.652	176.752	124.000	382.872	413.290	173.031	113.667	70.8
9	0.916	363.632	163.403	123.667	359.806	412.076	164.007	115.000	70.7
10	0.837	398.657	194.303	113.000	402.456	452.066	221.015	110.333	72.4

$$y = 82.238 - 15.078x_1 + 0.034x_2$$
$$+0.007x_3 - 0.004x_4 - 0.015x_5$$
$$+0.006x_6 - 0.014x_7 - 0.047x_8. \quad (3)$$

The R^2 of constructed multiple linear regression equation is the error caused by linear fitting. The closer this value is to 1, the more accurate the prediction is. The R^2 of this multiple linear regression equation is 0.984, which indicates that this equation has high prediction accuracy.

It can be seen from Eq. (3) that the noise of the tire is determined by the absolute value a_i of the polynomial coefficient and the average value of the grounding characteristic parameters $\bar{x}_i$. When

analysing the contribution of grounding characteristic parameters to noise, both of them should be considered together. Therefore, this paper evaluates the contribution of noise value by the product of the coefficients of different grounding regions (polynomial coefficients) of the regression equation and the average value of the corresponding grounding characteristic parameters. The results are shown in Table 4.

Table 4. Contribution of ground deformation parameters

I	II	III	IV
$a_4 \cdot \bar{x}_4$	$a_5 \cdot \bar{x}_5$	$a_6 \cdot \bar{x}_6 + a_7 \cdot \bar{x}_7$	$a_8 \cdot \bar{x}_8$
0.49	5.50	4.96	5.36
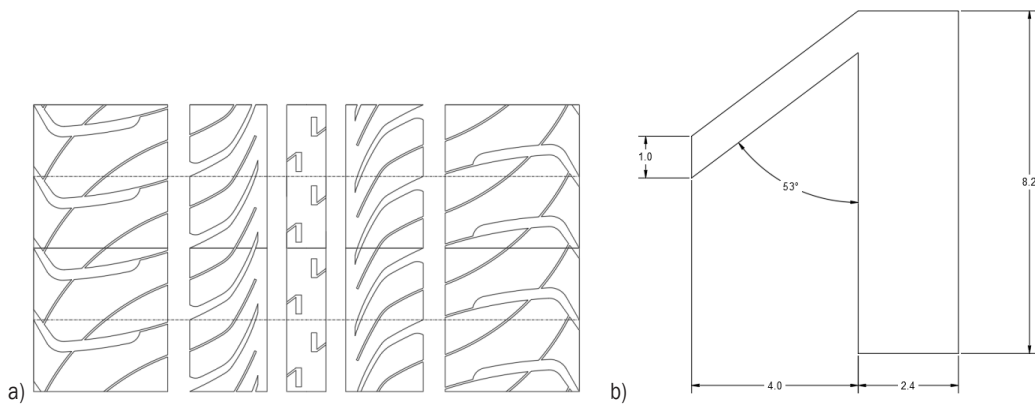
Fig. 7. Tire pattern bionic variant; a) tread pattern; and b) side branch structure and parameters
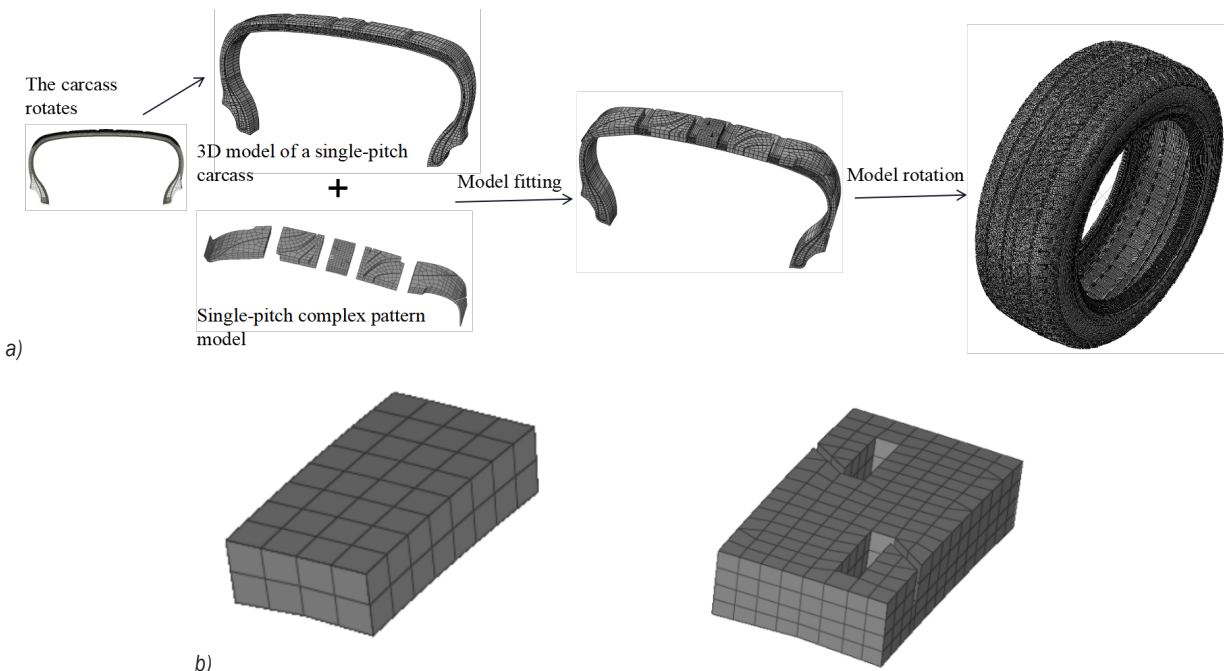
Fig. 8. Finite element modelling process and single-pitch centre block structure model of raw and bionic tires; a) finite element modeling process; and b) model of the structure of the centre block of the single pitch of the original and bionic tires

As shown in Table 4, it can be seen that the contribution degree to tire noise is from high to low, and the centre area (III), inner tire shoulder area (V), inner transition area (IV), and outer tire shoulder area (I). Therefore, in order to reduce noise, we can start with the pattern design in the central area.

3 DESIGN AND ANALYSIS OF TIRE PATTERN BIONIC VIBRATION AND NOISE REDUCTION

3.1 Tire Pattern Bionic Vibration and Noise Reduction Design

The vibration characteristics of tires are an important part of the NVH performance of vehicles. Inspired by the domestic cat's paw pad to weaken the impact from the ground through swinging deformation, reducing the radial vibration characteristics of tires is an important means of vibration and noise reduction of vehicles. Moreover, through the previous research of the research group, the side branch pipe structure has a certain weakening effect on the pipe resonance noise of the pattern, can simultaneously improve the anti-skid performance of the tire, and can synergistically improve the comprehensive performance of the tire [23].

As shown in Fig. 7, the 205/55R16 passenger car tire is taken as the research object, and the dislocation side branch pipe groove pattern is arranged in the central area of the tread, so as to achieve the characteristics of vibration reduction by imitating the swing deformation of the cat palm pad. Therefore, the finite element analysis model of the tire is established as shown in Fig. 8. During modelling, the Yeoh model is used for rubber material, Rebar is used for cord description, and there are 2141 nodes and 1998 units in a two-dimensional matrix. See Zhou et al. [24] and Chen et al. [25] for specific material properties and finite element type settings.

3.2 Verification of the Finite Element Model

3.2.1 Tire Static Ground Pressure Distribution Test

The modelling method of the finite element analysis model in this paper has been verified by a large number of experiments [24] and [25]. To verify the validity of the finite element model in this paper, the pressure distribution test system is used to test the grounding pressure when the tire is inflated to 0.21 MPa and loaded to 3800 N. Fig. 10 shows the pressure comparison between the test and simulation analysis results; it can be seen that the distribution of

the test and simulation grounding pressure has a good consistency.

3.2.2 Tire Stiffness Test

An MTM-2 comprehensive strength tester is used to test the stiffness of the 205/55R16 radial passenger car tire in accordance with GB/T23663-2009 [26]. The test and simulation results of tire squat, static loading radius, and radial stiffness under different test conditions are shown in Tables 5 and 6, from which it can be seen that the subsidence, static loading radius, and radial stiffness of the test and simulation have good consistency.

3.2.3 Tire Modal Test

To further verify the validity of the finite element model, the mode tests are carried out on tires using dynamic testing equipment from LMS 24-Channel Data Source Collector. The sampling frequency of the instrument is 25600 Hz. The modal analysis software is LMS Test. Lab. Acceleration sensor for the US PCB company triaxial acceleration sensor 356A34. The impact hammer is the US PCB 086C02 impact hammer. The test tire is put in the free suspension state, and 24 measuring points are evenly arranged on the tire surface. The physical diagram of the tire test is shown in Fig. 9.

Fig. 9. *Actual pattern of the modal test*

In this test, the hammer method is used for excitation, point-by-point excitation is used, and the

acceleration sensor is used to measure the response signal. The excitation and response signals are amplified and input into the dynamic analyser, and the transfer function in the range of 0 Hz to 320 Hz is obtained through analysis and processing. Each measuring point is hammered three times, and the transfer function of this point is obtained after a linear average, and then the first six radial natural frequencies and vibration modes of the tire under a free mounting state are obtained.

The Lanczos method in Abaqus is used in the tire free mode finite element analysis to calculate the first six radial natural frequencies and vibration modes in the free state of the tire and compare them with the test mode. The results are shown in Table 7.

It can be seen from Table 7 that the relative error between the first six natural frequencies of the tire obtained from simulation and the first six natural frequencies of the tire obtained from testing is less than 10 %. Its error meets the analysis requirements. s can be seen from Fig. 11, the simulation and test of the first sixth-order modal mode of the tire have strict symmetry and good consistency, which further verifies the accuracy of the finite element model.

The main reasons for the error are as follows:
1. A variety of rubber materials and steel wire materials are used in the tire, and the distribution of the materials in the simulation analysis is slightly different from that of the actual tire.
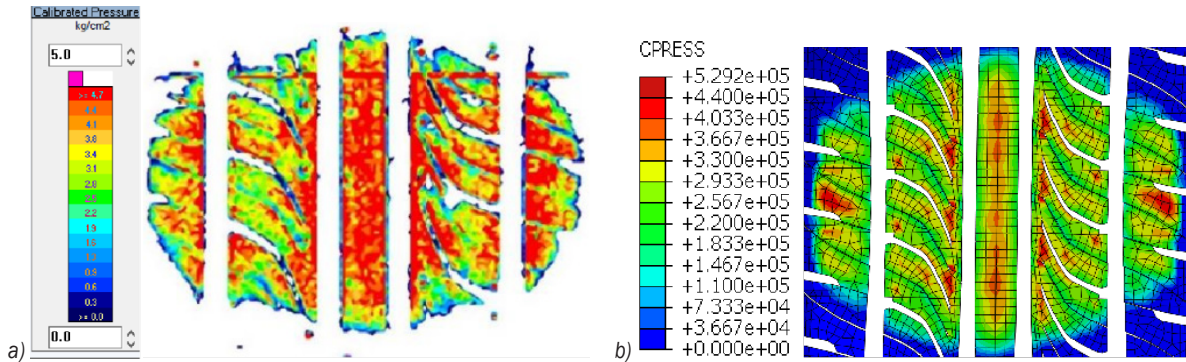
Fig. 10. *Comparison of tire grounding pressure distribution;*
a) test the ground pressure distribution; and b) simulate the ground pressure distribution

Table 5. *Comparison of test and simulation results of tire squat and static loading radius under different test conditions*

Test conditions	Test value				Simulation value			
	210 kPa		250 kPa		210 kPa		250 kPa	
	Squat [mm]	Static loading radius [mm]	Squat [mm]	Static loading radius [mm]	Squat [mm]	Static loading radius [mm]	Squat [mm]	Static loading radius [mm]
123 kg	6.01	308.14	5.49	309.01	6.48	309.47	5.98	309.97
246 kg	12.28	301.87	11.13	303.37	12.17	303.78	11.62	304.33
369 kg	18.06	296.09	16.29	298.21	18.28	297.67	16.99	298.96

Table 6. *Comparison between test value and simulation value of tire stiffness*

	Load [kg]	210 kPa			250 kPa		
		Test value [N/mm]	Simulation value [N/mm]	Error [%]	Test value [N/mm]	Simulation value [N/mm]	Error [%]
Radial stiffness	123	200.57	186.02	7.25	219.56	201.57	8.19
	246	196.32	198.09	-0.90	216.60	207.47	4.22
	369	200.23	197.82	1.20	221.99	212.84	4.12

Table 7. *Comparison of tire natural frequency test and simulation results*

Order	1	2	3	4	5	6
Test value [Hz]	59.625	100.102	110.391	138.711	165.304	191.455
Simulation value [Hz]	64.442	90.894	113.06	135.64	158.46	181.09
Error [%]	7.47	9.2	2.42	2.21	4.14	5.41
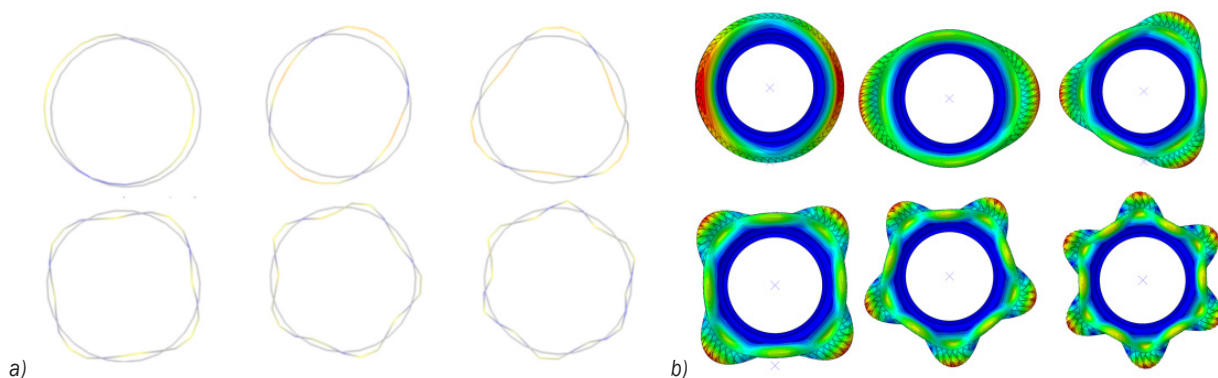
Fig. 11. *Test test and numerical calculation of the first 6th order modal mode of the tire; a) test results; and b) simulation results*

2. The simulation analysis simplified some of the small tread grooves and simplified the rim of the tire, resulting in a different stiffness and mass of the simulated tire than the actual tire.
3. While the modal analysis is based on linear assumptions, the tire material is highly nonlinear.

3.3 Development of a Model for Analysing Tire Vibration and Noise

The tire vibration and noise simulation model are shown in Fig. 12. The observation points for the arranged sound pressure measurement refer to GB/T3767-2016. A semi-circular bell jar with a radius of one metre is built around the tire. Nineteen acoustic observation points are defined on the semi-circular bell jar, and a plane is built at the bottom of the tire to simulate the road surface sound reflection. Through analysis and calculation, it can be concluded that the curve trends in the frequency band obtained from the 19 acoustic observation points are roughly the same, but the sound pressure values are different. The total sound pressure level of tire vibration noise is obtained by the A-weighted superposition of the 19 acoustic observation points, and this value is used as the evaluation index of tire vibration noise.
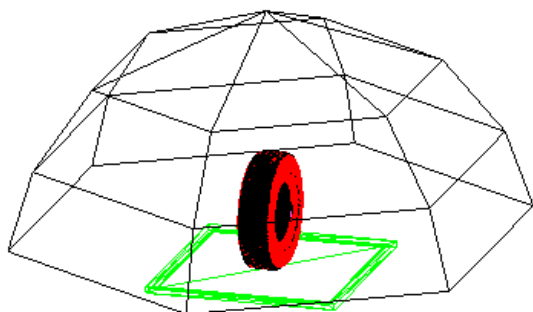
Fig. 12. *Tire vibration and noise simulation model*

4 RESULT ANALYSIS AND DISCUSSION

4.1 Comparison and Analysis of Tire Ground Strain

The strain distribution of the original tire and the bionic tire in X and Y directions under 70 km/h steady state rolling is obtained through finite element analysis, and the results are shown in Fig. 13, from which it can be seen that the bionic tire with staggered branch pipe pattern in the central area of the tread changes the symmetry of the strain distribution in the X and Y directions compared with the original tire, and the asymmetric deformation will form the swinging deformation in the X and Y directions during the rolling process of the tire. Therefore, the swing characteristics of the grounding deformation of the cat's paw pad can be achieved by arranging the misplaced side branch pipes in the central area of the tire pattern.

4.2 Results and Analysis of the Radial Excitation Force

The 70 km/h display rolling calculation is carried out for the tire, and the radial excitation force of the tire after steady rolling is extracted. The comparison of the radial excitation force between the original tire and the bionic tire in the time domain is shown in Fig. 14. Through the comparison, it can be seen that the peak radial excitation force of the bionic tire is reduced, and the range of radial excitation force fluctuations is reduced, thereby reducing the vibration phenomenon during the driving of the tire. It shows that the misplaced side branch pipe structure on the tire tread realizes the function of the bionic cat claw and reduces the radial excitation force to the tire from the ground.
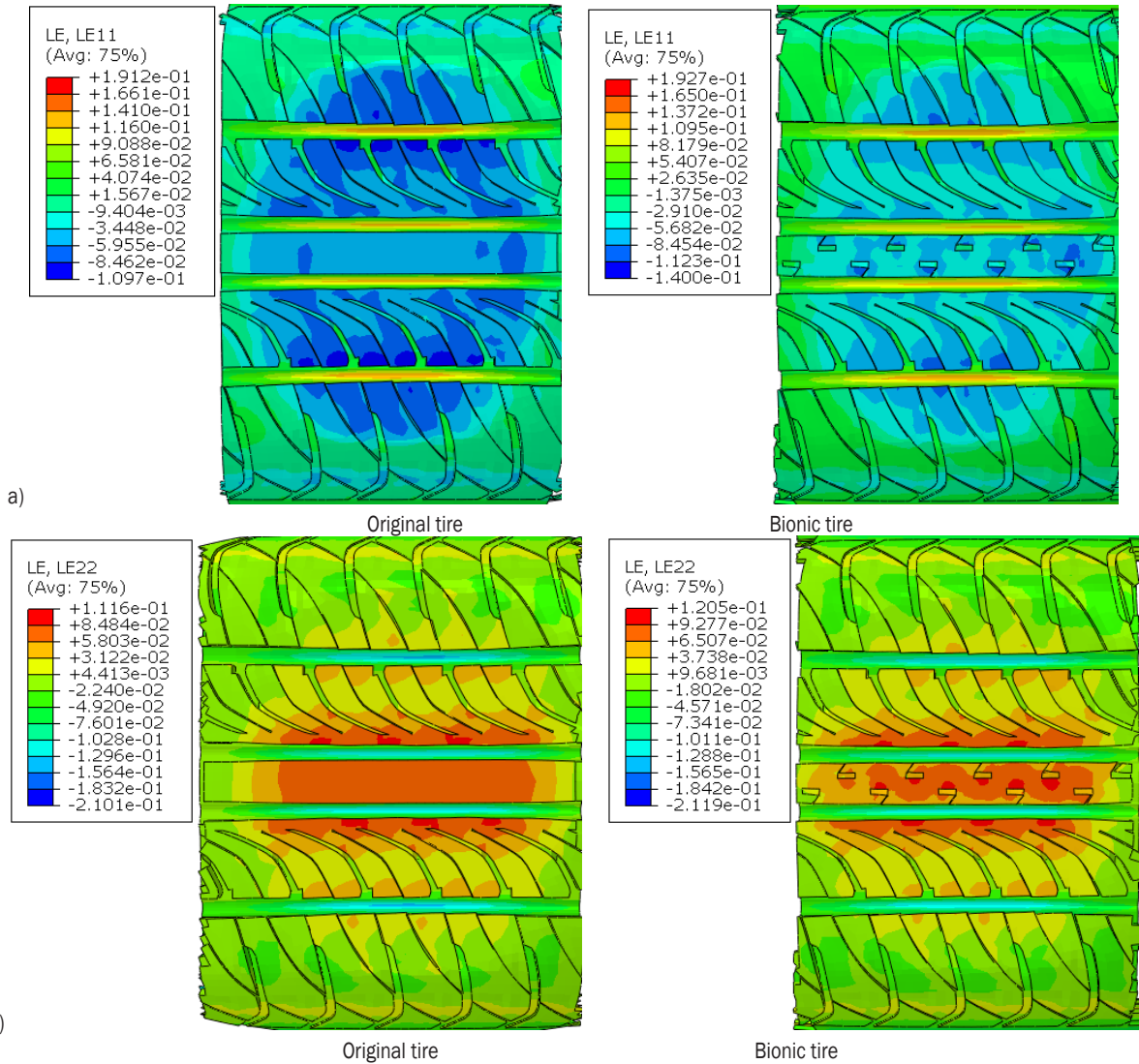
Fig. 13. *Strain distribution in the X and Y directions of the ground area when the two tires are rolling steadily; a) strain distribution in the X direction of both tire; and b) strain distribution in the Y direction of the two tires*
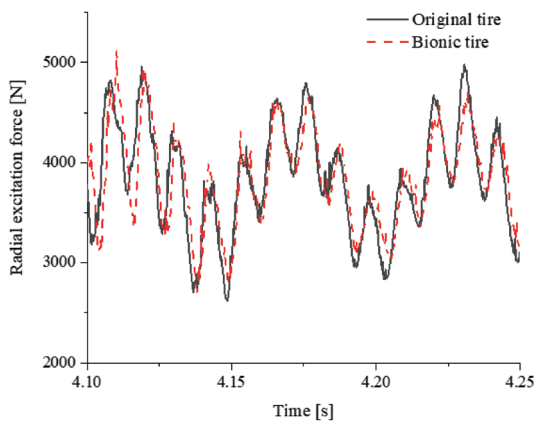
Fig. 14. *Comparison diagram of time domain characteristics of two types of tires subjected to ground radial excitation forces*
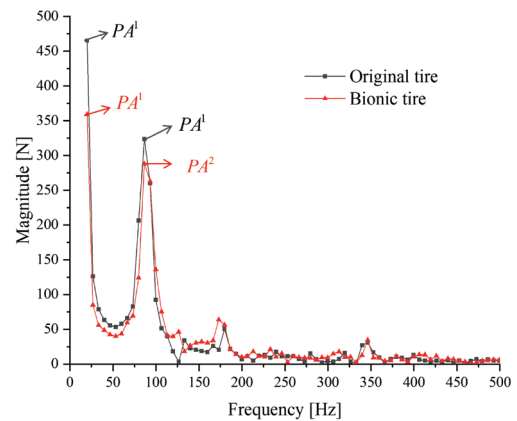
Fig. 15. *Comparison of frequency domain characteristics of amplitude of ground radial excitation force on two types of tires*

To further clarify the difference between the radial excitation force of the original tire and the bionic tire, fast Fourier transform (FFT) is performed on the radial excitation force in the time domain to obtain the amplitude-frequency characteristics of the radial excitation force in the frequency domain. The results are shown in Fig. 15. As the sound below 20 Hz cannot be heard by human ears, and the tire vibration noise is mainly concentrated below 500 Hz [27] and [28], this paper takes 20 Hz to 500 Hz as the frequency range for analysis. In Fig. 15, PA^1 is the peak amplitude 1, and PA^2 is the peak amplitude 2. At PA^1 (20 Hz), the amplitude value of the radial excitation force on the bionic tire is 22.16 % lower than that on the original tire, and at PA^2 (87 Hz) it is 8.53 % lower. It shows that the tread pattern tire with cat claw function has an obvious vibration reduction effect.

4.3 Numerical Analysis of Vibration and Noise and Discussion of Results

In order to analyse the vibration and noise characteristics of bionic tires with misaligned side branch structures in the tread centre, the vibration and noise analysis model established in this paper and the analysis process in literature [9] and [24] are used to analyse the tire vibration and noise. The vibration noise of the original tire and the bionic tire at 20 Hz to 500 Hz is shown in Fig. 16.
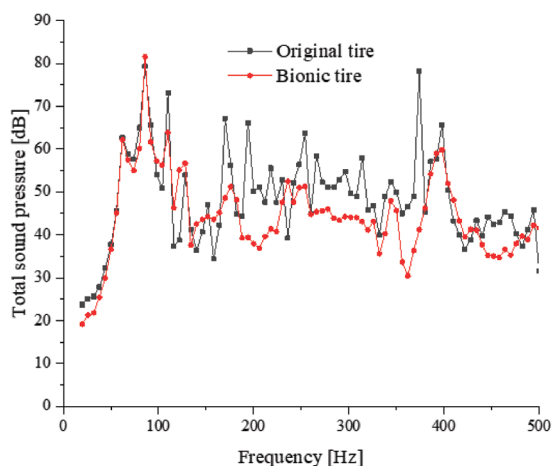
Fig. 16. *Comparison of the total sound pressure level of the two types of tires*

The sound pressure level of the bionic tire is lower than the total sound pressure level of the original tires in the whole frequency band, especially at 374 Hz, which is reduced from 78.25 dB to 41.20 dB, which is 47.35 %. The total noise value of the original tire is 64.02 dB and the noise value of the bionic tire is 62.86 dB by A-weighted superposition of the noise value in the 20 Hz to 500 Hz frequency band, which further shows that the bionic tire with misaligned sidewall structure has a good noise reduction effect.

It can be seen from Table 8 that in the comparison of the vibration and noise characteristics between the original tire and the bionic tire, the bionic tire has a better inhibition effect on the impact load from the ground during driving. This pattern design has a good effect on the vibration and noise reduction of the tire, which verifies the feasibility of bionic vibration and noise reduction.

Table 8. *Comparison of amplitude and noise values of the two types of tires*

Tire type	PA^1	PA^2	Total sound pressure level [dB]
Original tire	465.37	323.65	64.02
Bionic tire	362.24	296.05	62.86

5 CONCLUSION

1. Through the grounding mechanical test on the paw pad of the domestic cat, it is found that the left and right swing grounding characteristics of the paw pad of the domestic cat during walking is one of the main ways to achieve the effect of vibration reduction and silence during walking.
2. By analysing the grounding characteristic parameters of ten tires, it is concluded that the tire centre area has the greatest impact on tire noise. On this basis, combined with the vibration reduction principle of the left and right swing of the cat paw pad during walking, the staggered side branch pipe groove is set in the centre of the tire to achieve the vibration reduction characteristics of the swing of the cat paw pad.
3. The bionic tire can significantly reduce the amplitude and fluctuation range of the ground radial excitation force, thereby effectively reducing the vibration noise in the low frequency band, and improving the vibration noise characteristics of the tire.

5 ACKNOWLEDGEMENTS

8 REFERENCES

[1] Sandberg, U., Ejsmont, J.A. (2002). *Tyre/Road Noise Reference Book*. INFORMEX, Kisa.

[2] Diaz, C.G., Kindt, P., Middelberg, J., Vercammen, S., Thiry, C., Close, R., Leyssens, J. (2016). Dynamic behaviour of a rolling tyre: Experimental and numerical analyses. *Journal of Sound and Vibration*, vol. 364, p. 147-164, **DOI:10.1016/j. jsv.2015.11.025**.

[3] EUR-Lex (2014). European Parliament and Council, Regulation (EU) no 540/2014 on the sound level of motor vehicles and of replacement silencing systems and amending directive 2007/46/EC and repealing directive 70/157/EEC, *Official Journal of the European Union*, L 158/131, p. 131-195.

[4] Sen, H. (2013). Present status and prospect on vehicle NVH technology. *Automobile Parts*, vol. 7, p. 78-81, **DOI:10.19466/j. cnki.1674-1986.2013.05.019**. (in Chinese)

[5] Abouel-Seoud, S. (2019). Tire and engine sources contribution to vehicle interior noise and vibration exposure levels. *Archives of Acoustics*, vol. 44, no. 2, p. 201-214, **DOI:10.24425/ aoa.2019.126366**.

[6] Ji, L., Bolton, S.J. (2015). Coupling mechanism analysis of structural modes and sound radiations of a tire tread band based on the S-mode technique. *Applied Acoustics*, vol. 99, p. 161-170, **DOI:10.1016/j.apacoust.2015.06.013**.

[7] Zuo, S.G., Xin, T.I., Zeng, X., Xu-Dong, W. U. (2014). Analysis of structural vibration noise characteristics of rolling tire. *Journal of Jiamusi University (Natural Science Edition)*, vol. 32, no. 2, p. 161-165. (in Chinese)

[8] Mohammadi, S., Ohadi, A. (2021). A novel approach to design quiet tires, based on multi-objective minimization of generated noise. *Applied Acoustics*, vol. 175, art. ID 107825 **DOI:10.1016/j.apacoust.2020.107825**.

[9] Pei, X., Wang, G., Zhou, H., Zhao, F., Yang, J. (2016). Influence of tread structure design parameters on tire vibration noise. *Proceedings of SAE-China Congress 2015: Selected Papers. Lecture Notes in Electrical Engineering*, vol. 364, p. 325-338, **DOI:10.1007/978-981-287-978-3_30**.

[10] Zhang, D., Zhu, Z. H., Jian, L., Chen, H., Chen, X. (2012). Effect of carcass structure on noise of semi-steel radial tire. *The 16th China Tire Technology Seminar*, p. 138-140.

[11] Ling, S., Yu, F., Sun, D., Sun, G., Xu, L. (2021). A comprehensive review of tire-pavement noise: Generation mechanism, measurement methods, and quiet asphalt pavement. *Journal of Cleaner Production*, vol. 287, art. ID 125056, **DOI:10.1016/j.jclepro.2020.125056**.

[12] Coulmance, M., Gahéry, Y., Massion, J., Swett, J.E. (1979). The placing reaction in the standing cat: a model for the study of posture and movement. *Experimental Brain Research*, vol. 37, p. 265-281, **DOI:10.1007/BF00237713**.

[13] Zhang, X., Yang, J., Yu, H. (2012). Mechanical buffering characteristics of feline paw pads. *Journal of Biomedical Engineering*, vol. 29, no. 6, p. 1098-1104. (in Chinese)

[14] Kruger, K.M., Graf, A., Flanagan, A., McHenry, B. D., Altiok, H., Smith, P.A., Krzak, J.J. (2019). Segmental foot and ankle kinematic differences between rectus, planus, and cavus foot types. *Journal of Biomechanics*, vol. 94, p. 180-186, **DOI:10.1016/j.jbiomech.2019.07.032**.

[15] Wang, G., Tong, X., Dong, Z., Haiqing, X.U. (2016). Study on relationship between grounding characteristics and crown temperature field of radial tire. *China Rubber Industry*, vol. 63. (in Chinese)

[16] Su, B. (2009). Cooper bionic honeycomb tire. *Rubber Technology Market*, vol. 7, no. 10, p. 14. (in Chinese)

[17] Chen, L., Zhao, F., Wang, G.L., Yang, J., Zhou, H.C. ,Wan, Z.J. (2019). Tire vibration noise study of radial truck tire based on a new non-natural equilibrium design. *Journal of Vibration Engineering*, vol. 37, no. 1, p. 23-31, **DOI:10.16731/j. cnki.1671-3133.2019.01.005**.

[18] Zhang, R., Li, G., Qiao, Y., Jiang, L., Li, J. (2019). Analysis for effect of tire tread element of imitation reindeer plantar morphology on tire anti-skid performance. *Transactions of the Chinese Society of Agricultural Engineering*, vol. 35, no. 7, p. 47-53, **DOI:10.11975/j.issn.1002-6819.2019.07.006**.

[19] Zhou, L., Wang, H. (2013). Imitation octopus sucker-type tire tread pattern design and finite element analysis. *Journal of Xi'an University of Technology*, vol. 29, no. 2, p. 228-232, **DOI:10.19322/j.cnki.issn.1006-4710.2013.02.021**.

[20] Morris, A., Erles, K., Maddox, T.W. (2018). Displacement of an ununited medial humeral condylar ossification centre in the cat. *Veterinary and Comparative Orthopaedics and Traumatology*, vol. 31, no. 2, p. 153-157, **DOI:10.3415/VCOT-17-06-0084**.

[21] Zhang, Z.Y. (2016). 2016 China Tire German Test [J/OL], from *https://www.autohome.com.cn/drive/201608/891160-2. html*, accessed on 2020-09-10.

[22] Liang, C. (2013). Research on evaluation system and method of comprehensive grounding performance of radial tire. *Jiangsu University*. (in Chinese)

[23] Wang,G. L., Zhou, H.C.,Yang, J. (2014). Simulation analysis of the influence of branch pipe on tire noise and anti-water skiing performance. *Journal of System Simulation*, vol. 26, no. 3, p. 675-681, **DOI:10.16182/j.cnki.joss.2014.03.005**. (in Chinese)

[24] Zhou, H., Li, H., Liang, C., Zhang, L., Wang, G. (2021). Relationship between tire ground characteristics and vibration noise. *Strojniški vestnik - Journal of Mechanical Engineering*, vol. 67, no. 1-2, p. 11-27, **DOI:10.5545/sv-jme.2020.6946**.

[25] Chen, L., Zhao, F., Wang, G.L. , Yang, J., Zhou, H.C., Wan, Z.J. (2015). Tire vibration noise study of radial truck tire based on a new non-natural equilibrium design. *Journal of Vibration Engineering*, vol. 28, no. 05, p. 800-808, **DOI:10.16385/j.cnki. issn.1004-4523.2015.05.016**.

[26] GB/T 23663-2009. Test method of automobile tyre longitudinal and lateral stiffness from *https://www.auto-testing.net/news/show-105200.html*, accessed on 2021-03-10. (in Chinese)

[27] Heckl, M. (1986). Tyre noise generation. *Wear*, vol. 113, no. 1, p. 157-170, **DOI:10.1016/0043-1648(86)90065-7**.

[28] Bai, S., Xu, X., Liu, X. (2013). Vehicle panel acoustic contribution analysis and tests for noise reduction. *Journal of Vibration and Shock*, vol. 32, no. 24, p. 204-208, **DOI:10.13465/j.cnki.jvs.2013.2**.